Volume 16, Issue 1, 162507 (1-10)

International Journal of Nano Dimension (IJND)

https://dx.doi.org/10.57647/j.ijnd.2025.1601.07

Camellia sinensis mediated Zinc Ferrite nanoparticles synthesis and their application in thiamethoxam degradation

Jayanta Das[1], Nirmalendu Das[2*], Krishna Chandra Das [3], Siddhartha Sankar Dhar[4]

[1]*Cachar Advisory Centre, Tocklai Tea Research Institute, Cachar, Assam, India.*
[2]*Department of Chemistry, Patharkandi College, Karimganj, Assam, India.*
[3]*Department of Chemistry, G.C College, Cachar, Assam, India.*
[4]*Department of Chemistry, NIT, Silchar, Cachar, Assam, India.*

[*]**Corresponding author:** nirmaldas1987@gmail.com

Original Research

Received:
29 August 2024
Revised:
11 October 2024
Accepted:
15 October 2024
Published online:
10 January 2025

Abstract:

In this work $ZnFe_2O_4$ nanoparticles (NPs) were synthesized via green method using shoots of *Camellia sinensis* (*C. sinensis*). The crystalline nature of $ZnFe_2O_4$ NPs (CS-$ZnFe_2O_4$ NPs) was confirmed by X-ray diffraction (XRD) and selected area electron diffraction (SAED) study. Further characterizations were done using UV-Vis spectroscopy, FTIR spectroscopy, SEM-EDX, TEM, XPS, and VSM. The size of synthesized NPs was calculated to be 14.4 nm which presented spherical morphology along with some irregular shaped particles. The synthesized nanoparticles showed excellent catalytic activity towards degradation of a widely used pesticide, Thiamethoxam under solar radiation. Thiamethoxam got 89% degraded within 60 minutes of experimental time. This work is carried out for the first time where zinc ferrite nanoparticles have been synthesized using *C. sinensis* followed by the application towards Thiamethoxam (THIA) degradation.

Keywords: *C.sinensis*; CS-$ZnFe_2O_4$ NPs; Degradation; Green synthesis; Thiamethoxam (THIA); Zinc Ferrite

1. Introduction

In the recent years, there has been an alarming increase in the use of pesticides in agricultural practices. To meet the growing demand of the increasing population, the usage of pesticides by agricultural industries has risen to peak levels [1]. Pesticides, in general, are used for pest control, but a considerable quantity often accumulates in the soil and is eventually discharged into nearby water bodies [2]. These compounds unknowingly pose serious threats to human civilization. Among various types of pesticides, Thiamethoxam (THIA) is one of the most widely used neonicotinoid varieties [3, 4]. THIA has become a preferred pesticide because of its unique biological and chemical properties. It is used against a wide variety of sucking and biting pests, including helopeltis, mites, aphids, termites, and a few species of Lepidoptera, as either a foliar or soil treatment [5, 6]. However, some of its properties, such as low soil sorption and high leaching capability, make it a potential source of contamination for both surface and groundwater [6]. Studies have shown that THIA is toxic, carcinogenic, and difficult to mineralize under ordinary circumstances, posing a continuous threat to human health and the ecological system [3, 5]. Therefore, it has become urgently necessary to develop an efficient method to combat this problem. Reports indicate that very few studies have been conducted to degrade or destroy THIA by any means. Some of the investigated methods for THIA degradation include degradation by reactive oxygen species [5], ozonation [3], TiO_2 particles [6], Fe co-doped N-TiO_2 / Ti nanotubes [4], zero-valent metals [7], and semiconductor oxides [8]. Nanocomposites offer a cost-effective, high-performance, and biodegradable solution for efficient adsorption in environmental remediation

efforts [9]. Similarly, superparamagnetic nanocomposites such as $MgFe_2O_4$@CeO_2 have shown promising photocatalytic performance, demonstrating effective reusability and potential applications in wastewater treatment [10]. Recent advancements in green synthesis approaches, particularly using plant extracts, have garnered attention due to their environmental friendliness and ability to produce nanoparticles with diverse applications in catalysis, photocatalysis, antibacterial treatments, colorimetric sensing, environmental remediation, and dye degradation [11–14] owing to their biocompatibility, cost-effectiveness, and multifunctionality. For instance, green-synthesized α-Mn_2O_3 nanoparticles exhibit strong photocatalytic efficiency and antibacterial activity, offering potential in both environmental and biomedical applications [15]. Furthermore, zinc ferrite nanoparticles, such as $Cu_{0.25}Zn_{0.75}Fe_2O_4$, have been synthesized through green methods, providing magnetic properties, high stability, and reusability, making them effective and environmentally friendly photocatalysts for pollutant removal [16]. Spinel nanoparticles, such as $NiFe_2O_4$@$ZnMn_2O_4$ and $Zn_{0.5}Ni_{0.5}FeCrO_4$, demonstrate remarkable versatility in various applications due to their unique properties. $NiFe_2O_4$@$ZnMn_2O_4$ magnetic nanocomposites, featuring a distinct spinel structure, exhibit strong catalytic activity in the microwave-assisted synthesis of tetrahydropyrimidine and polyhydroquinoline derivatives, with the added advantage of easy recovery and reusability through magnetic separation [17]. Similarly, $Zn_{0.5}Ni_{0.5}FeCrO_4$ spinel nanoparticles showcase excellent ferromagnetic properties and photocatalytic efficiency, making them highly effective for the degradation of persistent organic pollutants such as 4-nitrophenol and aniline in wastewater remediation [18].

In recent times, the use of spinel ferrites in the photocatalytic treatment of organic contaminants has become a trending research area. Spinel ferrites are considered as one of the important functional materials because of their soft magnetic properties and suitable band gap [12–19]. Spinel ferrite nanoparticles (NPs) have garnered enormous attention due to their promising applications in data storage, drug delivery, batteries, medical diagnosis, gas sensors, and photocatalysis [20–30]. Doping with various cations such as Al^{3+}, Cr^{3+}, Ti^{4+}, Co^{2+}, Mn^{3+}, Zr^{4+}, Zn^{2+}, and Co_{2+} has been shown to alter physical properties like magneto-crystalline anisotropy and magnetic parameters [31]. Among spinel ferrites, zinc ferrite NPs have particularly attracted researchers' attention due to their unique chemical stability, moderate saturation magnetization, and high electromagnetic performance [32]. Most synthesis methods for zinc ferrite NPs involve chemical and physical techniques, including coprecipitation, thermal decomposition, hydrothermal, microemulsion, sol-gel, solid-state reactions, mechanical activation, solvothermal, ultrasonic cavitation, probe sonication, and electrochemical synthesis [27, 33–45]. However, these methods have drawbacks such as environmental threats, labor-intensive processes, complex procedures, and high costs. Only a few studies have reported the green synthesis of spinel ferrite NPs, specifically zinc ferrite NPs [14, 37, 46–49]. The synthesis of nanoparticles using leaf extracts has garnered significant interest recently due to its cost-effectiveness and eco-friendly nature [50, 51].

This study primarily focuses on the green synthesis of zinc ferrite nanoparticles ($ZnFe_2O_4$ NPs) using the leaf extract of *Camellia sinensis* (*C. sinensis*) as a reducing and stabilizing agent. The synthesized green zinc ferrite NPs were then applied as photocatalytic agents for the degradation of Thiamethoxam (THIA). *C. sinensis* is widely known for its rich variety of chemical constituents. The leaves of *C. sinensis* are reported to contain approximately 4,000 bioactive chemicals, with polyphenols accounting for one-third of them. These phytocompounds are known to act as reducing, chelating and stabilizing agents in the green synthesis of nanomaterials [52–55]. According to the literature survey, no work has been conducted so far to degrade THIA using *C. sinensis*-mediated zinc ferrite nanoparticles (CS-$ZnFe_2O_4$ NPs). This study is likely the first to demonstrate the photocatalytic degradation of THIA using green CS-$ZnFe_2O_4$ NPs.

2. Experimental

2.1 Materials

Two leaves and a bud of *C.sinensis* were selectively collected from the experimental plot of Tocklai, Tea Research Institute, Silcuri, Cachar, Assam, India. Reagents zinc nitrate hexahydrate ($Zn(NO_3)_2.6H_2O$, $\geq$ 96% and Iron (II) sulphate heptahydrate ($FeSO_4.7H_2O$, $\geq$ 95% were purchased from Merck while Thiamethoxam (THIA, $\geq$ 98%) was purchased from Sigma Aldrich. All the reagents are of analytical grade and are used without any further purification. Deionised water was used throughout the experimental study.

2.2 Preparation of tea leaves extract

Selectively plucked young shoots of *C. sinensis* were chopped into fine pieces using a kitchen knife. The chopped pieces were then air-dried for about 2 hours. Subsequently, 80 g of the chopped pieces were boiled in 500 mL of deionized water at 80 ^{O}C for approximately 90 minutes until reddish liquor was formed. The resulting liquor was cooled, centrifuged, and filtered twice through Whatman filter paper No. 1 to obtain the extract. The extract was then refrigerated for further use.

2.3 Green synthesis of pure CS-$ZnFe_2O_4$ NPs

In a typical process, 9.4 g of $FeSO_47H_2O$ was dissolved in 50 ml of preheated tea leaf extract maintained at 80 ^{O}C. This was followed by the gradual addition of 5 g of $Zn(NO_3)2•6H_2O$, and the mixture was magnetically stirred for about 1 hour to obtain a mass of brown-colored slurry. The resulting mass was dried in an oven at 60 ^{O}C and then annealed at 1000 ^{O}C for 1 hour to obtain a brick-red powder, which was finely ground to produce $ZnFe_2O_4$ nanoparticles (NPs), as shown in Fig. 1.

2.4 Mechanism of synthesis of CS-$ZnFe_2O_4$ NPs

The possible mechanism for the synthesis of CS-ZnFe2O4 nanoparticles (NPs) is represented in Fig. 2. The phytochemicals in general are pronounced for their potential reduction

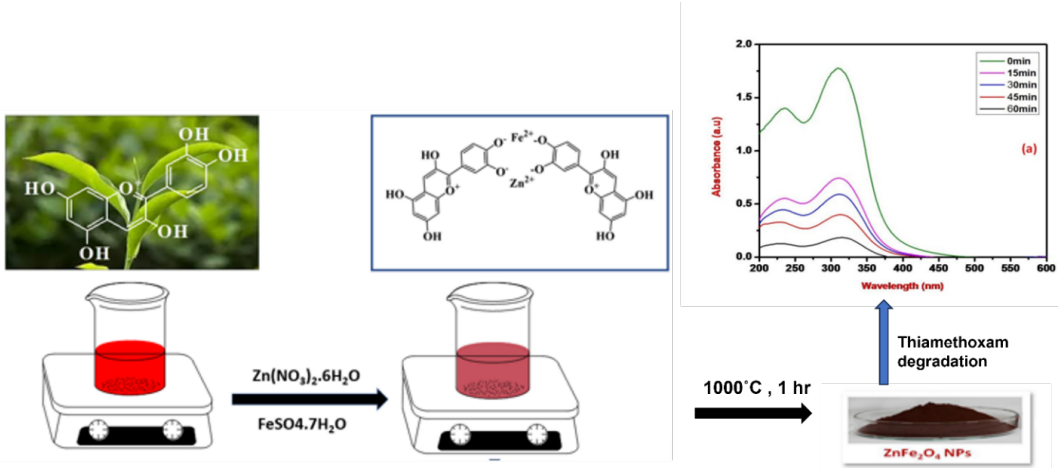

Figure 1. Produce $ZnFe_2O_4$ nanoparticles (NPs).

ability to synthesis variety of metal nanoparticles [12–14]. But here in this work the phenolic compounds in *C. sinensis* interact with precursor zinc and iron ions, leading to the formation of a chelate-like system [32, 52–55]. The formation of CS-$ZnFe_2O_4$ NPs occurs via the decomposition of the zinc-iron polyphenol chelate during calcination at an elevated temperature (1000 ^{O}C).

2.5 Characterisation of CS-$ZnFe_2O_4$ NPs

Preliminary characterization of CS-$ZnFe_2O_4$ nanoparticles (NPs) was conducted using various analytical techniques. UV-visible spectroscopy (UV-Vis) was performed with a Cary 300 model to analyze the optical properties. X-ray diffraction (XRD) analysis was carried out using an X-PERT3 MRD XL to assess the crystallinity of the NPs. Fourier transform infrared spectroscopy (FTIR) analysis was conducted with an IMPACT 410 model to identify the presence of phytochemicals involved in the nanoparticle synthesis. Scanning electron microscopy-Energy dispersive X-ray (SEM-EDX) analysis was performed using a Jeol 6390LA/OXFORD XMX N model to determine the morphology and elemental composition of the synthesized nanoparticles. Transmission electron microscopy-Selected area electron diffraction (TEM-SAED) analysis was used to examine the size and to confirm the crystallinity of the nanoparticles. X-ray photoelectron spectroscopy (XPS) analysis was conducted to investigate the chemical states of the primary constituent elements in the prepared sample. Finally, the magnetic properties of the NPs were studied using a Vibrating Sample Magnetometer (VSM) with a Lake Shore 4700 model.

2.6 Degradation experiment

The degradation of THIA was carried out using CS-$ZnFe_2O_4$ NPs as a photocatalyst under solar light irradiation. In the degradation experiment 50 mg of CS-$ZnFe_2O_4$ NPs were finely dispersed in 10 mg/L solution of THIA under direct sunlight with constant stirring. The degradation progress was monitored using UV-Vis spectrophotometer at the maximum absorbance of THIA (λ_{max} = 311nm) at a time interval of 15 minutes for a contact time of 60 minutes. The degradation efficiency (η) CS-$ZnFe_2O_4$ NPs for the experiment has been calculated using the equation 1.The degradation of THIA was carried out using CS-$ZnFe_2O_4$

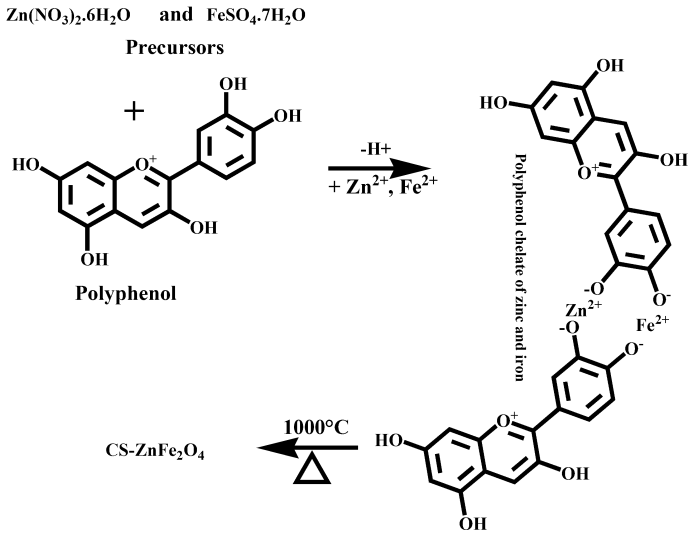

Figure 2. Mechanism of synthesis of CS-ZnFe2O4 NPs.

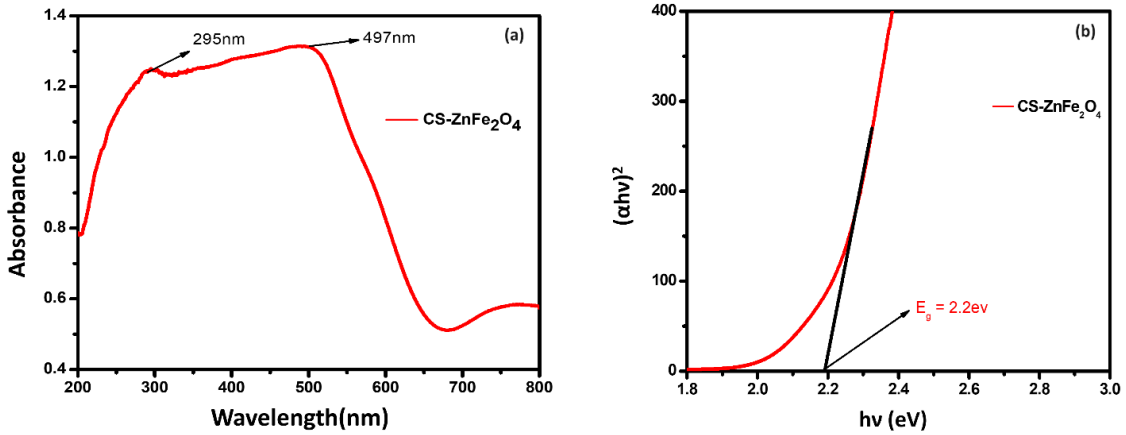

Figure 3. (a) Absorption spectrum, and (b) Calculation of band gap (E_g) of CS-$ZnFe_2O_4$ NPs.

NPs as a photocatalyst under solar light irradiation. In the degradation experiment 50 mg of CS-$ZnFe_2O_4$ NPs were finely dispersed in 10 mg/L solution of THIA under direct sunlight with constant stirring. The degradation progress was monitored using UV-vis spectrophotometer at the maximum absorbance of THIA (λ_{max} = 311nm) at a time interval of 15 minutes for a contact time of 60 minutes. The degradation efficiency (η) CS-$ZnFe_2O_4$ NPs for the experiment has been calculated using the equation 1.

$$\eta = \frac{A_0 - A_t}{A_0} \quad (1)$$

where A_0 and A_t represent the initial and final absorbance of THIA respectively.

Similar degradation experiment was conducted in dark in presence and absence of CS-$ZnFe_2O_4$ NPs but not as such noticeable results obtained. Self-degradation of THIA also did not take place when the solution was exposed to direct sunlight [5].

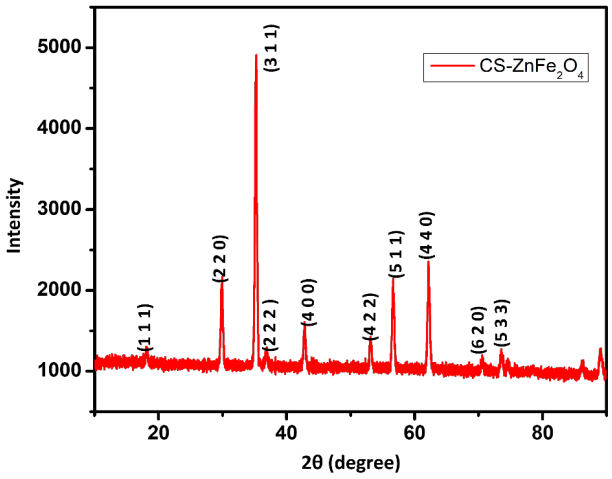

Figure 4. XRD pattern of CS-ZnFe2O4 NPs.

3. Results and discussion

3.1 UV-Vis study

The UV-Vis spectrum (Fig. 3a) of green synthesized CS-$ZnFe_2O_4$ reflected two major peaks, one with less intensity 295 nm and another with high intensity 497 nm [18]. The optical band gap (E_g) of CS-$ZnFe_2O_4$ was calculated from the Tauc's plot of $(\alpha h\nu)^2$ versus $h\nu$ (Fig. 3b) following the literature method [56]. The extrapolation of the linear region of the curve obtained to $(\alpha h\nu)^2 = 0$ gave the value E_g equals to 2.2 eV. The band gap value obtained here lies in the range for pure ferrite NPs [18, 45] and hence as synthesized CS-$ZnFe_2O_4$ NPs are expected for better photocatalytic performance.

3.2 XRD study

The XRD pattern of photosynthesized CS-$ZnFe_2O_4$ NPs is shown in Fig. 4. The appearance of distinctive diffraction peak at 2θ = 18.17, 29.97, 35.24, 36.98, 42.88, 53.08, 56.42, 62.17, 70.61 and 73.64 corresponding to (111), (220), (311), (222), (400), (422), (511), (440), (620) and (533) crystal planes with an excellent match with JCPDS card No. 1-1108 indicate highly crystalline nature. In fact, the highest peak at 35.24 corresponding to (311) plane confirms the synthesis of $ZnFe_2O_4$ NPs [57, 58]. The crystalline size of the particle is calculated using Scherrer's equation [59], and is found to be around 10 nm. The absence of secondary phase in pattern further assures the presence of pure single phase cubic spinel $ZnFe_2O_4$ NPs.

3.3 FT-IR study

The FTIR spectrum (Fig. 5.) of CS - $ZnFe_2O_4$ NPs reflected two sharp peaks 558 cm^{-1} and 433 cm^{-1} which are attributed to the stretching vibration of Zn - O bond in tetrahedral sites and Fe - O bond in octahedral sites. Appearance of such peaks confirmed the formation spinel $ZnFe_2O_4$ as the range 500 – 600 cm^{-1} and 450 – 385 cm^{-1} is usually corresponded to tetrahedral metal-oxygen and octahedral metal-oxygen stretching vibrations of spinel metal ferrites [18, 56]. The involvement of phenolic compounds in the synthesis of $ZnFe_2O_4$ is evidenced from the appearance of broad band 3406 cm^{-1} (H - bonded phenolic -OH) accompanied by relatively weak bands 1623 cm^{-1} (aromatic C=C stretching) and 1107 cm^{-1} (C - O stretching) [49].

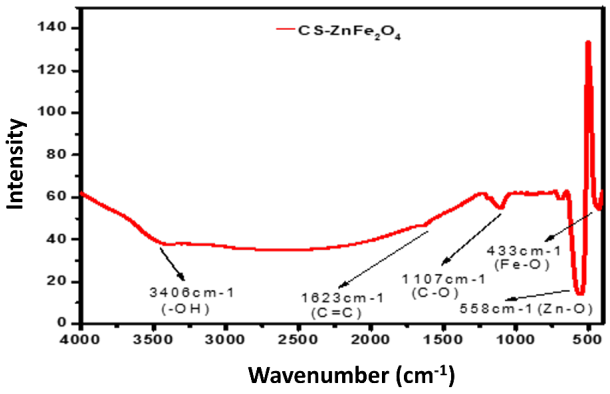

Figure 5. FTIR spectrum of CS-$ZnFe_2O_4$ NPs.

3.4 SEM – EDX study

The SEM images (Figs. 6a, and b) of as synthesized CS-$ZnFe_2O_4$ NPs shows the existence of agglomerated particles which are mainly a mixture of porous flakes and irregular spheres. The agglomeration among the particles might be due to the coordination between the phenolic –OH groups and zinc ions [48]. The qualitative information obtained from EDX spectrum (Fig. 6c) as expected shows the existence of intense peaks due to Zn (at 1.0 eV), Fe (at 6.5 eV) and O (at 0.5 eV) which signifies the purity of sample. Besides the two small peaks due to K (3.4 eV) and S (2.4 eV) basically originated from the phytochemicals of *C. sinensis*. The table showing atomic and weight percentage of all the elements detected in EDX spectrum is attached in the Fig. 4c.

3.5 TEM study

The TEM images (Fig. 7a-d) revealed well-distributed particles, predominantly spherical, along with some irregularly shaped particles. The mean particle size was calculated to be 14.4 nm. The histogram distribution of particle size (Fig. 7e) indicated that the most particles fall within the range of 10-20 nm. The distinct concentric rings observed in the SAED pattern (Fig. 7f) confirm the polycrystalline nature of the prepared sample. Thus, the TEM study is consistent with the XRD results, further validating the successful synthesis of crystalline CS-$ZnFe_2O_4$.

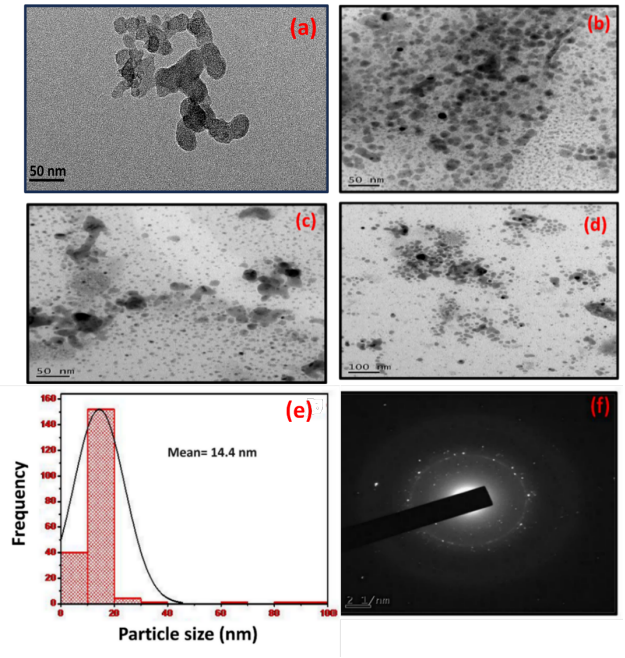

Figure 7. (a-d) TEM images, (e) Histogram distribution, and (f) SAED pattern of CS-$ZnFe_2O_4$ NPs.

3.6 XPS study

XPS study was conducted to know the surface composition and to assess the oxidation states of the primary constituent of CS-$ZnFe_2O_4$ NPs. XPS spectra of Zn 2p, Fe 2p, O 1s and C 1s are presented in the Fig. 7a-d. Zn 2p spectrum (Fig. 8a) shows the presence of two main peaks centering at 1044.7 eV and 1021.3 eV which are attributed mainly due Zn $2p_{1/2}$ and Zn $2p_{3/2}$ respectively revealing the existence of +2 oxidation state of Zn in the sample [30]. Fe 2p spectrum (Fig. 8b) of our sample displaying two peaks locating at 725.5 eV and 710.9 eV characterizes Fe $2p_{1/2}$

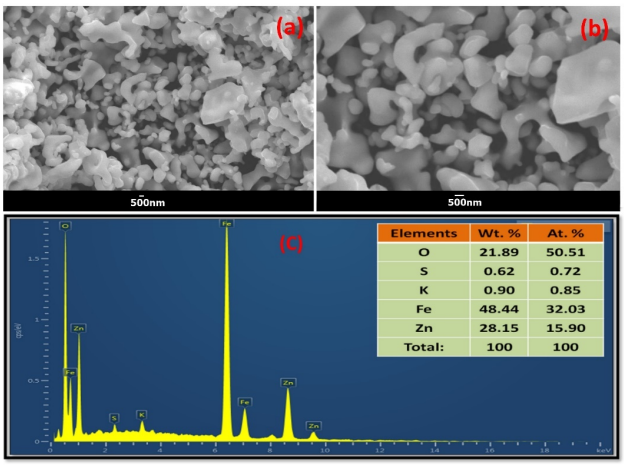

Figure 6. (a) and (b) SEM images, and (c) EDX spectrum of CS-$ZnFe_2O_4$ NPs.

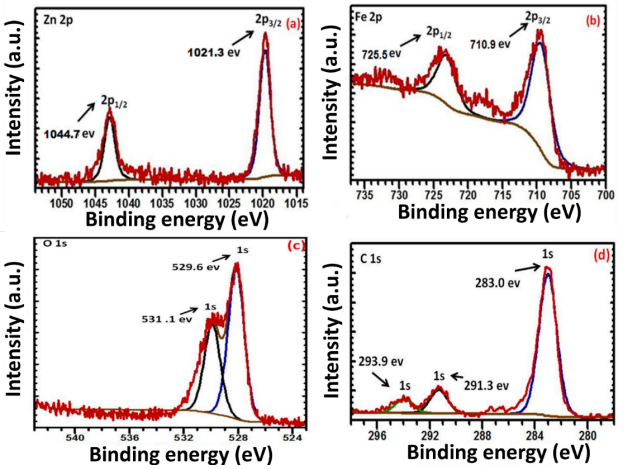

Figure 8. (a-d). XPS spectra of constituent elements present in CS-$ZnFe_2O_4$ NPs.

and Fe $2p_{3/2}$ due to the existence of +3 oxidation states [16, 60]. Besides, O 1s spectrum (Fig. 8 c) has been deconvulated into two peaks centering at 531.1 eV and 529.6 eV which shows the presence of lattice oxygen holding zinc and iron respectively (Zn-O and Fe-O) [21, 23, 55]. Lastly as expected adventitous C 1s spectrum (Fig. 8d) shows the presence of three peaks at 293.5 eV, 291.3 eV, and 283.0 eV due to the various carbon moeties originating from the phytocomponents of *C. sinensis*.

3.7 VSM study

The magnetic behavior of CS - $ZnFe_2O_4$ NPs was evaluated using vibration magnetometry whose result is presented in Fig. 9. The hysteresis curve as obtained clearly reveals the paramagnetic character [35], and this nature is usually obtained when the sample is calcined at a higher temperature [35, 42]. The saturation magnetization (Ms) and coercivity (Hc) value were calculated to be 1.37 emu/g and 20.79 Oe.

3.8 Photocatalytic efficiency

The degradation experiment revealed that CS-$ZnFe_2O_4$ NPs was successful to act as an efficient catalyst. The photocatalytic efficiency of CS-$ZnFe_2O_4$ NPs in degrading thiamethoxam (THIA) is evidenced by the decreasing peak intensity of THIA (Fig. 10a) at λ_{max} = 311 nm. It may be noted that the maximum peak intensity of THIA decreases with increasing time interval indicating continuation of the degradation process. The degradation percentage (η) reached to 89% within 60 minutes of experimental duration (Fig. 10b) and the peak of the THIA spectrum taken at 60 minutes (Fig. 10a) also got considerably flattened.

3.9 Degradation kinetics

The kinetics of degradation of THIA is tested employing first order kinetics using the equation 2 given below.

$$\ln A_t = -kt + \ln A_0 \qquad (2)$$

where k is the rate constant, A_0 and A_t are the initial and final absorbance.

The rate constant k for the degradation reaction is calculated from the equation 2. The linear relationship was obtained from the plot of $\ln[A_t]$ versus time (t)(Fig. 11a). The value

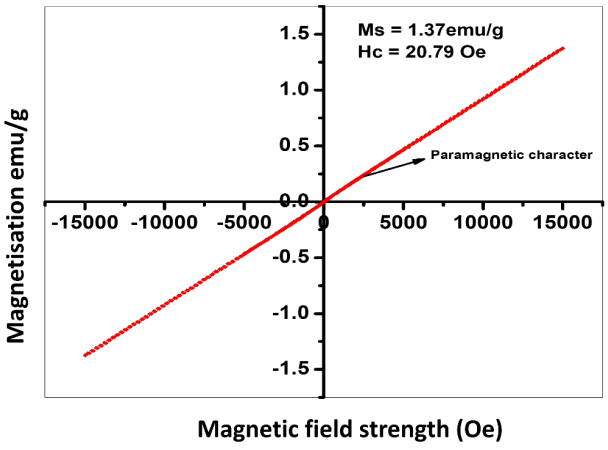

Figure 9. M-H loop of CS-$ZnFe_2O_4$ NPs.

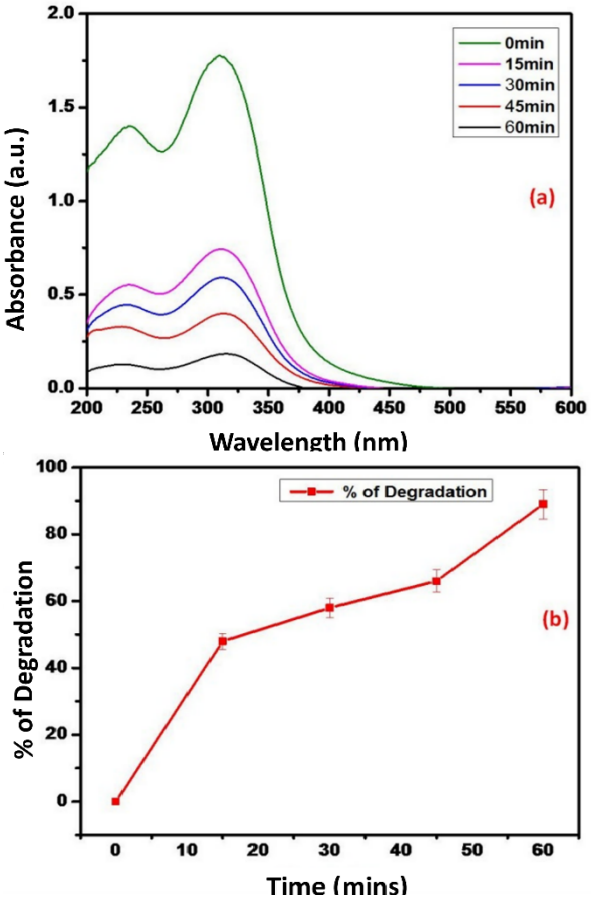

Figure 10. (a) UV-Vis spectral change, and (b) Change in degradation % of THIA.

of k which is also the slope of the line was calculated to be 0.04 min^{-1}. The plot A_t/A_0 versus time (t) (Fig. 11b) decreases with increasing time which also supports the increasing degradation percentage of THIA. As the plot of $\ln[A_t/A_0]$ versus time (t) is found to be linear with high correlation coefficient (R^2 = 0.950) as shown in Fig. 11c, the degradation process well fitted to first order kinetics. Therefore, the as synthesized CS-$ZnFe_2O_4$ NPs are proved to act as a one of the good photocatalyst in degradation of THIA.

3.10 Degradation mechanism

The photocatalytic degradation steps of THIA by CS-$ZnFe_2O_4$ NPs consisted of five steps. The mechanism of photodegradation of THIA by CS-$ZnFe_2O_4$ NPs is presented in Fig. 12.

3.11 Comparison of removal of THIA by other catalysts

The performance of THIA degradation using CS-$ZnFe_2O_4$ NPs was compared with some benchmark materials previously reported, as presented in Table 1. This work is considered superior in terms of utilizing green-synthesized CS-$ZnFe_2O_4$ NPs for the degradation experiment. Notably, this is likely the first study where green-synthesized $ZnFe_2O_4$ NPs have been effectively used in the photocatalytic degradation of THIA, achieving an 89% degradation rate within 60 minutes of contact time.

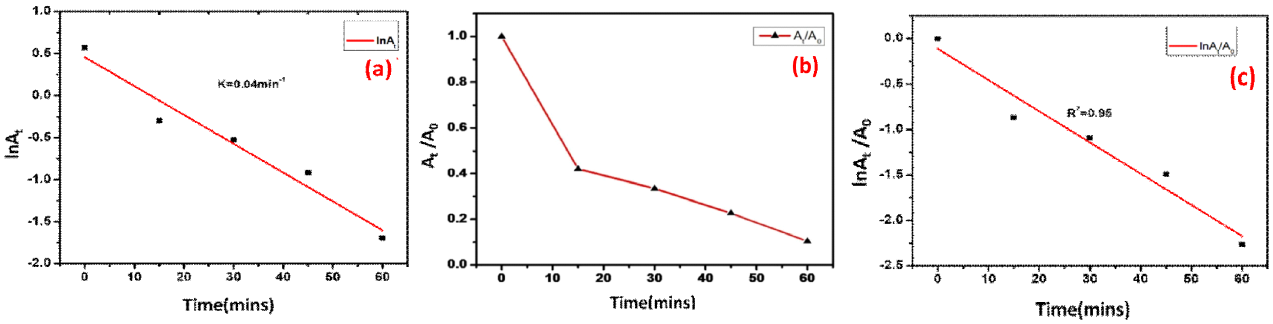

Figure 11. (a) Plot of lnAt versus time (t), (b) Plot A_t/A_0 versus time (t), and (c) Plot of $\ln A_t/A_0$ versus time (t).

Table 1. Comparison of degradation of THIA in presence of various catalysts and light .

Process	THIA conc.	Light source	Catalyst load (mg/L)	Time (min)	Degradation (%)	Ref.
TiO_2 as photocatalyst	115.2 μM	UV	2300	90	98	[5]
Ozonation	300 mg/L	No data	22.5	90	71	[3]
TiO_2 as photocatalyst	0.09 mM	UV	1000	21	89	[6]
Hexacyanoferrate NPs as adsorbent	50	Sunlight	60	No data	76-95	[1]
Zero-valent metals (Fe, Sn and Zn) exposed to ultrasonic irradiation	50	No data	5-25000	30	90	[7]
Fe-N-TiO_2/Ti nanotubes as photocatalyst	0.7	UV	No data	60	92	[4]
CS-$ZnFe_2O_4$ NPs as photocatalyst	10 mg/L	Sunlight	1000	60	89	Our work

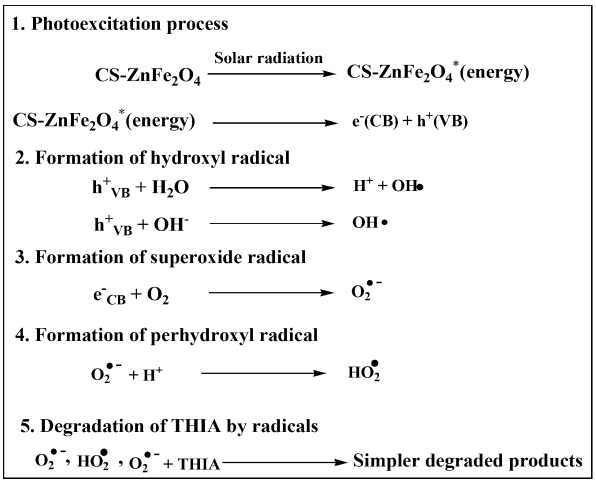

Figure 12. Mechanism of degradation of THIA.

4. Conclusion

The $ZnFe_2O_4$ nanoparticles (CS-$ZnFe_2O_4$ NPs) were successfully synthesized using a green method, employing *C. sinensis* as the reducing and stabilizing agent, making it one of the simplest synthesis routes. The NPs were thoroughly characterized using UV-Vis, PXRD, FTIR, SEM-EDX, TEM-SAED, XPS, and VSM confirming the successful synthesis of $ZnFe_2O_4$ NPs. As a photocatalyst, CS-$ZnFe_2O_4$ NPs demonstrated the ability to degrade the pesticide THIA by 89% within 60 minutes. Therefore, these eco-friendly synthesized CS-$ZnFe_2O_4$ NPs may be practically useful for removing similar organic contaminants from water systems worldwide.

Acknowledgement

The authors of this study acknowledge Sr. Advisory Officer and Sr. Technical Officer of Tocklai, Tea Research Institute, Cachar for their support to carry out the study conducted here. Our special thanks to CIF NIT Silchar, SAIF IIT Bombay, STIC Kerala, SAIF IIT Roorke and SAIC Tezpur University for providing us with the analytical data.

Authors contributions
Authors have contributed equally in preparing and writing the manuscript.

Availability of data and materials
The data used to support findings of this study are included within the article. The data that has been used is confidential.

Conflict of interests
The authors report no conflicts of interest. The authors alone are responsible for the content and writing the paper.

References

[1] M. Rani and U. Shanker. Removal of chlorpyrifos, thiamethoxam, and tebuconazole from water using green synthesized metal hexacyanoferrate nanoparticles. *Environ. Sci. Pollut. Res. Int.*, 25: 10878–10893, 2018.
DOI: https://doi.org/10.1007/s11356-018-1346-2.

[2] M. Rani and U. Shanker. Degradation of traditional and new emerging pesticides in water by nanomaterials: recent trends and future recommendations. *Int. J. Environ. Sci. Technol.*, 15:1347–1380, 2018.
DOI: https://doi.org/10.1007/s13762-017-1512-y.

[3] Q. Zhao, Y. Ge, P. Zuo, D. Shi, and S. Jia. Degradation of thiamethoxam in aqueous solution by ozonation: Influencing factors, intermediates, degradation mechanism and toxicity assessment. *Chemosphere*, 146:105–112, 2016.
DOI: https://doi.org/10.1016/j.chemosphere.2015.09.009.

[4] A. T. Maulidiyah, A. T. Nurwahidah, D. Wibowo, and M. Nurdin. Photoelectrocatalyst of fe co-doped n-tio$_2$ /ti nanotubes: Pesticide degradation of thiamethoxam under uv–visible lights. *Environ. Nanotechnol. Monit. Manag.*, 8:103–111, 2017.
DOI: https://doi.org/10.1016/j.enmm.2017.06.002.

[5] H. Yang, H. Liu, Z. Hu, J. Liang, H. Pang, and B. Yi. Consideration on degradation kinetics and mechanism of thiamethoxam by reactive oxidative species (ross) during photocatalytic process. *Chem. Eng. J.*, 245:24–33, 2014.
DOI: https://doi.org/10.1016/j.cej.2014.02.016.

[6] N. A. Mir, A. Khan, M. Muneer, and S. Vijayalakhsmi. Photocatalytic degradation of a widely used insecticide thiamethoxam in aqueous suspension of tio$_2$: adsorption, kinetics, product analysis and toxicity assessment. *Sci. Total Environ.*, 388:458–460, 2013.
DOI: https://doi.org/10.1016/j.scitotenv.2013.04.04.

[7] R. P. Lopes, A. P. F. M. de Urzedo, C. C. Nascentes, and R. Augusti. Degradation of the insecticides thiamethoxam and imidacloprid by zero-valent metals exposed to ultrasonic irradiation in water medium: electrospray ionization mass spectrometry monitoring. *Rapid Commun. Mass Spectrom.*, 22:3472–3480, 2008.
DOI: https://doi.org/10.1002/rcm.3749.

[8] J. Fenoll, I. Garrido, P. Hellín, P. Flores, and S. Navarro. Photodegradation of neonicotinoid insecticides in water by semiconductor oxides. *Environ. Sci. Pollut. Res.*, 22:15055–15066, 2015.
DOI: https://doi.org/10.1007/s11356-015-4721-2.

[9] B.F. Far, M.R. Naimi-Jamal, M. Jahanbakhshi, S. A. Khalafvandi, M. Alian, and D. R. Jahromi. Decontamination of congo red dye from aqueous solution using nanoclay/chitosan-graft-gelatin nanocomposite hydrogel. *J. Mol. Liq.*, 395:123839, 2024.
DOI: https://doi.org/10.1016/j.molliq.2023.123839.

[10] S.T. Fardood, F.Y. Zare, F. Moradnia, and A. Ramazani. Preparation, characterization and photocatalysis performances of superparamagnetic mgfe$_2$o$_4$@ceo$_2$ nanocomposites: Synthesized via an easy and green sol–gel method. *J. Rare Earth. In Press. Journal Pre-proof.*, 2024.
DOI: https://doi.org/10.1016/j.jre.2024.03.006.

[11] F. Moradnia, S. T. Fardood, A. Zarei, S. Heidarzadeh, A. Ramazani, and M. Sillanpää. Green synthesis of nickel oxide nanoparticles using plant extracts: an overview of their antibacterial, catalytic, and photocatalytic efficiency in the degradation of organic pollutants. *IJC.*, 14:1–24, 2024.
DOI: https://doi.org/10.1002/aoc.7315.

[12] T. Varadavenkatesan, V. Nagendran, R. Vinayagam, L. C. Goveas, and R. Selvaraj. Effective degradation of dyes using silver nanoparticles synthesized from thunbergia grandiflora leaf extract. *Bioresour. Technol. Rep.*, 27:101914, 2024.
DOI: https://doi.org/10.1016/j.biteb.2024.101914.

[13] R. Selvaraj, V. Nagendran, T. Varadavenkatesan, L. C. Goveas, and R. Vinayagam. Stable silver nanoparticles synthesis using tabebuia aurea leaf extract for efficient water treatment: A sustainable approach to environmental remediation. *Chem. Eng. Res. Des.*, 208: 456–463, 2024.
DOI: https://doi.org/10.1016/j.cherd.2024.07.012.

[14] R. Vinayagam, V. Nagendran, L. C. Goveas, M. K. Narasimhan, T. Varadavenkatesan, N. Chandrasekar, and R. Selvaraj. Structural characterization of marine macroalgae derived silver nanoparticles and their colorimetric sensing of hydrogen peroxide. *Mater. Chem. Phys.*, 313:128787, 2024.
DOI: https://doi.org/10.1016/j.matchemphys.2023.128787.

[15] S.T. Fardood, F. Moradnia, F. Y. Zare, S. Heidarzadeh, M. A. Majedi, A. Ramazani, and M. Sillanpää anad K. Nguyen. Green synthesis and characterization of α-mn$_2$o$_3$ nanoparticles for antibacterial activity and efficient visible-light photocatalysis. *Sci. Rep.*, 14:6755, 2024.
DOI: https://doi.org/10.1038/s41598-024-56666-2.

[16] M. T. Kiani, A. Ramazani, S. Rahmani, and S. T. Fardood. Green synthesis and characterisation of superparamagnetic cu$_{0.25}$zn$_{0.75}$fe$_2$o$_4$ nanoparticles and investigation of their photocatalytic activity. *Int. J. Environ. Anal. Chem.*, page 1–17, 2022.
DOI: https://doi.org/10.1080/03067319.2022.2076219.

[17] F. Moradnia, S. T. Fardood, and A. Ramazani. Green synthesis and characterization of nife$_2$o$_4$@znmn$_2$o$_4$ magnetic nanocomposites: An efficient and reusable spinel nanocatalyst for the synthesis of tetrahydropyrimidine and polyhydroquinoline derivatives under microwave irradiation. *Appl. Organomet. Chem.*, 38:e7315, 2023.
DOI: https://doi.org/10.1002/aoc.7315.

[18] S. T. Fardood, F. Moradnia, and T. M. Aminabhav. Green synthesis of novel zn$_{0.5}$ni$_{0.5}$fecro$_4$ spinel magnetic nanoparticles: Photodegradation of 4-nitrophenol and aniline under visible light irradiation. *Environ. Pollut.*, 358:124534, 2024.
DOI: https://doi.org/10.1016/j.envpol.2024.124534.

[19] P. Suppuraj, G. Thirunarayanan, M. Swaminathan, and I. Muthuvel. Facile synthesis of spinel nanocrystalline znfe$_2$o$_4$: Enhanced photocatalytic and microbial applications. *Mater. Sci. Appl. Chem.*, 34(1), 2017.
DOI: https://doi.org/10.1515/msac-2017-0001.

[20] R. Rahmayeni, Y. Oktavia, Y. Stiadi, S. Arief, and Z. Zulhadjri. Spinel ferrite of mnfe$_2$o$_4$ synthesized in piper betle linn extract media and its application as photocatalysts and antibacterial. *J. Dispersion Sci. Technol.*, 42:465–474, 2021.
DOI: https://doi.org/10.1080/01932691.2020.1721011.

[21] H. Xiang, X. Peng, D. Xu, X. Yang, G. Ren, Z. Zhang, Y. Zhong, and X. Wang. One-pot solvent-free synthesis of mgfe$_2$o$_4$ nanoparticles from ferrous sulfate waste. *Mater. Manuf. Processes.*, 35:590–597, 2020.
DOI: https://doi.org/10.1080/10426914.2020.1734617.

[22] S. O. Aisida, P. A. Akpa, I. Ahmad, M. Maaza, and F. I. Ezema. Influence of pva, pvp and peg doping on the optical, structural, morphological and magnetic properties of zinc ferrite nanoparticles produced by thermal method. *Physica. B, Condensed Matter.*, 571: 130–136, 2019.
DOI: https://doi.org/10.1016/j.physb.2019.07.001.

[23] P. Ajithkumar, S. Mohana, and S. Sumathi. Synthesis, characterization, optical and photocatalytic activity of yttrium and copper co-doped zinc ferrite under visible light. *J. Mater. Sci.: Mater. Electron.*, 31:1168–1182, 2020.
DOI: https://doi.org/10.1007/s10854-019-02628-8.

[24] M. Balasubramanian and K. R. Murali. Biosynthesis of zinc ferrite (znfe$_2$o$_4$) nanoparticles using flower extract of nyctanthes arbortristis and their photocatalytic activity. *Ferroelectrics.*, 555:1–14, 2020.
DOI: https://doi.org/10.1080/00150193.2019.1691381.

[25] M. Chandrika, A. V. Ravindra, C. Rajesh, S. D. Ramarao, and S. Ju. Studies on structural and optical properties of nano znfe$_2$o$_4$ and znfe$_2$o4-tio$_2$ composite synthesized by co-precipitation route. *Mater. Chem. Phys.*, 230:107–113, 2019.
DOI: https://doi.org/10.1016/j.matchemphys.2019.03.059.

[26] G. K. Dinesh, S. Anandan, and T. Sivasankar. Synthesis of fe/zno composite nanocatalyst and its sonophotocatalytic activity on acid yellow 23 dye and real textile effluent. *Clean Technol. Environ. Policy.*, 2016.
DOI: https://doi.org/10.1007/s10098-016-1117-z.

[27] K. C. Das and S. S. Dhar. Rapid catalytic degradation of malachite green by mgfe$_2$o$_4$ nanoparticles in presence of h$_2$o$_2$. *J. Alloys Compd.*, 828:154462, 2020.
DOI: https://doi.org/10.1007/s10098-016-1117-z.

[28] K. K. Kefeni, B. B. Mamba, and T. A. M. Msagati. Application of spinel ferrite nanoparticles in water and wastewater treatment: A review. *Sep. Purif. Technol.*, 188:399–422, 2017.
DOI: https://doi.org/10.1016/j.seppur.2017.07.015.

[29] L.-Z. Liu Chen Y.-J. Wang P.J. H.-J. Zhang, F.-N. Meng. Highly sensitive h_2s sensor based on solvothermally prepared spinel $znfe_2o_4$ nanoparticles. *J. Alloys Compd.*, 764:147–154, 2018.
DOI: https://doi.org/10.1016/j.jallcom.2018.06.052.

[30] M. Wang, Y. Huang, X. Chen, K. Wang, H. Wu, N. Zhang, and H. Fu. Synthesis of nitrogen and sulfur co-doped graphene supported hollow $znfe_2o_4$ nanosphere composites for application in lithium-ion batteries. *J. Alloys Compd.*, 691:407–415, 2017.
DOI: https://doi.org/10.1016/j.jallcom.2016.08.285.

[31] M. Alimoradi, M. Yousefi, B. Sadeghi, M. M. Amini, and A. Abbasi. Structural and magnetic behavior of $baal_xcr_yfe_{11}o_{19}$ (x + y = 1) hexagonal ferrites. *J. Supercond. Nov. Magn.*, 32:2533–2538, 2019.
DOI: https://doi.org/10.1007/s10948-018-4980-5.

[32] K. Kombaiah, J. J. Vijaya, L. J. Kennedy, and M. Bououdina. Studies on the microwave assisted and conventional combustion synthesis of hibiscus rosa-sinensis plant extract based $znfe_2o_4$ nanoparticles and their optical and magnetic properties. *Ceram. Int.*, 42:2741–2749, 2016.
DOI: https://doi.org/10.1016/j.ceramint.2015.11.003.

[33] Y. Yao, J. Qin, Y. Cai, F. Wei, F. Lu, and S. Wang. Facile synthesis of magnetic $znfe_2o_{4-}$ reduced graphene oxide hybrid and its photo-fenton-like behavior under visible irradiation. *Environ. Sci. Pollut. Res.*, 21:7296–7306, 2014.
DOI: https://doi.org/10.1007/s11356-014-2645-x.

[34] G. Fan, Z. Gu, L. Yang, and F. Li. Nanocrystalline zinc ferrite photocatalysts formed using the colloid mill and hydrothermal technique. *Chem. Eng. J.*, 155:534–541, 2009.
DOI: https://doi.org/10.1016/j.cej.2009.08.008.

[35] J. Vilcakova P. Urbánek M. Machovsky M. Masař M. Holek R. S. Yadav, I. Kuřitka. Structural, magnetic, optical, dielectric, electrical and modulus spectroscopic characteristics of $znfe_2o_4$ spinel ferrite nanoparticles synthesized via honey-mediated sol-gel combustion method. *J. Phys. Chem. Solids.*, 110:87–99, 2017.
DOI: https://doi.org/10.1016/j.jpcs.2017.05.029.

[36] J. Kaur and M. Kaur. Facile fabrication of ternary nanocomposite of $mgfe_2o_4$ tio_2@go for synergistic adsorption and photocatalytic degradation studies. *Ceram. Int.*, 45:8646–8659, 2019.
DOI: https://doi.org/10.1016/j.ceramint.2019.01.185.

[37] K. Kombaiah, J. J. Vijaya, L. J. Kennedy, and M. Bououdina. Studies on the microwave assisted and conventional combustion synthesis of hibiscus rosa-sinensis plant extract based $znfe_2o_4$ nanoparticles and their optical and magnetic properties. *Ceram Int.*, 42:2741–2749, 2016.
DOI: https://doi.org/10.1016/j.ceramint.2015.11.003.

[38] F. Liu, K. Zhou, Q. Chen, A. Wang, and W. Chen. Application of magnetic ferrite nanoparticles for removal of cu(ii) from copper-ammonia wastewater. *J. Alloys Compd.*, 773:140–149, 2019.
DOI: https://doi.org/10.1016/j.jallcom.2018.09.240.

[39] A. Asadipour E. Kargar M. Malakootian, A. Nasiri. Facile and green synthesis of $znfe_2o_4$@cmc as a new magnetic nanophotocatalyst for ciprofloxacin degradation from aqueous media. *Process Saf. Environ. Prot.*, 129:138–151, 2019.
DOI: https://doi.org/10.1016/j.psep.2019.06.022.

[40] R. Rameshbabu, N. Kumar, A. Karthigeyan, and B. Neppolian. Visible light photocatalytic activities of $znfe_2o_4$/zno nanoparticles for the degradation of organic pollutants. *Mater. Chem. Phys.*, 181:106–115, 2016.
DOI: https://doi.org/10.1016/j.matchemphys.2016.06.040.

[41] N. M. Mahmoodi. Zinc ferrite nanoparticle as a magnetic catalyst: Synthesis and dye degradation. *Mater. Res. Bull.*, 48:4255–4260, 2013.
DOI: https://doi.org/10.1016/j.materresbull.2013.06.070.

[42] V. I. Popkov, V. P. Tolstoy, and V. G. Semenov. Synthesis of phase-pure superparamagnetic nanoparticles of znfe2o4 via thermal decomposition of zinc-iron layered double hydroxysulphate. *J. Alloys Compd.*, 813:152179, 2020.
DOI: https://doi.org/10.1016/j.jallcom.2019.152179.

[43] X. Zhang, Z. Chen, C. Wu, J. Zhang, and F. Wang. Solvothermal synthesis of spinel $znfe_2o_4$ nanoparticles with enhanced infrared radiation property. *Chem. Phys. Lett.*, 732:136647, 2019.
DOI: https://doi.org/10.1016/j.cplett.2019.136647.

[44] M. Sivakumar, A. Towata, K. Yasui, T. Tuziuti, and Y. Iida. A new ultrasonic cavitation approach for the synthesis of zinc ferrite nanocrystals. *Curr. Appl. Phys.*, 6:591–593, 2006.
DOI: https://doi.org/10.1016/j.cap.2005.11.068.

[45] B. S. Surendra, T. R. Shashi Shekhar, M. Veerabhadraswamy, H. P. Nagaswarupa, S. C. Prashantha, G. C. Geethanjali, and C. Likitha. Probe sonication synthesis of $znfe_2o_4$ nps for the photocatalytic degradation of dyes and effect of treated wastewater on growth of plants. *Chem. Phys. Lett.*, 745:137286, 2020.
DOI: https://doi.org/10.1016/j.cplett.2020.137286.

[46] M. Sriramulu, D. Shukla, and S. Sumathi. Aegle marmelos leaves extract mediated synthesis of zinc ferrite: Antibacterial activity and drug delivery. *Mater. Res. Express.*, 5:115404, 2018.
DOI: https://doi.org/10.1088/2053-1591/aadd88.

[47] T. F. Saeid, M. Ferzaneh, M. Miad, A. Zolfa, F. Vahid, and G. Sara. Biosynthesis of $mgfe_2o_4$ magnetic nanoparticles and its application in photo-degradation of malachite green dye and kinetic study. *Nanochem Res.*, 4:86–93, 2019.
DOI: https://doi.org/10.22036/ncr.2019.01.010.

[48] B. S. Surendra, H. P. Nagaswarupa, M. U. Hemashree, and J. Khanum. Jatropha extract mediated synthesis of $znfe_2o_4$ nanopowder: Excellent performance as an electrochemical sensor, uv photocatalyst and an antibacterial activity. *Chem. Phys. Lett.*, 739:136980, 2020.
DOI: https://doi.org/10.1016/j.cplett.2019.136980.

[49] N. Matinise, K. Kaviyarasu, N. Mongwaketsi, S. Khamlich, L. Kotsedi, N. Mayedwa, and M. Maaza. Green synthesis of novel zinc iron oxide (znfe2o4) nanocomposite via moringa oleifera natural extract for electrochemical applications. *Appl. Surf. Sci.*, 446:66–73, 2018.
DOI: https://doi.org/10.1016/j.apsusc.2018.02.187.

[50] I. Singh, T. Mazhar, V. Shrivastava, and Singh R. Tomar. Bio-assisted synthesis of bi-metallic (ag-zn) nanoparticles by leaf extract of azadirachta indica and its antimicrobial properties. *Int. J. Nano Dimens.*, 13:168–178, 2022.
DOI: https://doi.org/10.22034/ijnd.2022.686558.

[51] P. Kumari, H. Kumar, I. Kumar, M. Sohail, K. Pratap Singh, and K. Prasad. Biosynthesized zinc oxide nanoparticles control the growth of aspergillus flavus and its aflatoxin production. *Int. J. Nano Dimens.*, 10:320–329, 2019.
DOI: https://doi.org/20.1001.1.20088868.2019.10.4.1.8.

[52] M. Tariq, A. Naveed, and A. K. Barkat. The morphology, characteristics, and medicinal properties of camellia sinensis tea. *J. Med. Plant Res.*, 4:2028–2033, 2010.
DOI: https://doi.org/10.5897/jmpr10.010.

[53] B. E. Sumpio, A. C. Cordova, D. W. Berke-Schlessel, F. Qin, and Q. H. Chen. Green tea, the 'asian paradox,' and cardiovascular disease. *J. Am. Coll. Surg.*, 202:813–825, 2006.
DOI: https://doi.org/10.1016/j.jamcollsurg.2006.01.018.

[54] C. Cabrera, R. Artacho, and R. Giménez. Beneficial effects of green tea–a review. *J. Am. Coll. Nutr.*, 25:79–99, 2006.
DOI: https://doi.org/10.1080/07315724.2006.10719518.

[55] J. Das and S. S. Dhar. Synthesis of sno_2 quantum dots mediated by camellia sinensis shoots for degradation of thiamethoxam. *Toxicol. Environ. Chem.*, 102:186–196, 2020.
DOI: https://doi.org/10.1080/02772248.2020.1776285.

[56] S.T. Fardood, S. Ganjkhanlu, F. Moradnia, and A. Ramazani. Green synthesis, characterization, and photocatalytic activity of superparamagnetic $mgfe_2o_4$@$znal_2o_4$ nanocomposites. *Sci.Rep.*, 14:16670, 2024.
DOI: https://doi.org/10.1038/s41598-024-67655-w.

[57] K. C. Das and S. S. Dhar. Removal of cadmium (ii) from aqueous solution by hydroxyapatite-encapsulated zinc ferrite (hap/$znfe_2o_4$) nanocomposite: kinetics and isotherm study. *Environ. Sci. Pollut. Res.*, 27:37977–37988, 2020.
DOI: https://doi.org/10.1007/s11356-020-09832-8.

[58] M. Madhukara Naik, H. S. Bhojya Naik, G. Nagaraju, M. Vinuth, H. Raja Naika, and K. Vinu. Green synthesis of zinc ferrite nanoparticles in limonia acidissima juice: Characterization and their application as photocatalytic and antibacterial activities. *Microchem. J.*, 146:1227–1235, 2019.
DOI: https://doi.org/10.1016/j.microc.2019.02.059.

[59] M.T. Kiani, A. Ramazani, and S. T. Fardood. Green synthesis and characterization of $ni_{0.25}zn_{0.75}fe_2o_4$ magnetic nanoparticles and study of their photocatalytic activity in the degradation of aniline. *Appl. Organomet. Chem.*, 37:e7053, 2023.
DOI: https://doi.org/10.1002/aoc.7053.

[60] H. Song, L. Zhu, Y. Li, Z. Lou, M. Xiao, and Z. Ye. Preparation of $znfe_2o_4$ nanostructures and highly efficient visible-light-driven hydrogen generation with the assistance of nanoheterostructures. *J. Mater. Chem. A. Materials for Energy and Sustainability*, 3: 8353–8360, 2015.
DOI: https://doi.org/10.1039/c5ta00737b.